

SENSITIVITY KERNELS FOR HELIOSEISMIC TRAVEL TIMES IN SPHERICAL GEOMETRY – PRELIMINARY RESULTS

M. Roth¹, L. Gizon¹, and A. C. Birch²

¹Max-Planck-Institut für Sonnensystemforschung, 37191 Katlenburg-Lindau, Germany

²North West Research Associates Inc., CoRA Division, Boulder, CO 80301, USA

ABSTRACT

We discuss the problem of the computation of three-dimensional Frechet kernels in spherical geometry for use in time-distance helioseismology. In particular, we investigate the computation of the kernels that give the linear sensitivity of travel times to internal flows. Simple tests have been performed in the case of uniform rotation.

1. INTRODUCTION

Time-distance helioseismology, after Duvall et al. [1], is a technique of local helioseismology. Unlike global helioseismology, time-distance helioseismology enables us to make three-dimensional maps of the solar interior (see [2] and references therein). The basic measurements in time-distance helioseismology are acoustic-wave travel times. The travel time $\tau(\mathbf{r}_1|\mathbf{r}_2)$ for waves propagating from point \mathbf{r}_1 to point \mathbf{r}_2 on the solar surface is measured from the temporal cross-covariance between the oscillation signals measured at \mathbf{r}_1 and \mathbf{r}_2 .

Here we study the sensitivity of the travel-time difference $\delta\tau(\mathbf{r}_1|\mathbf{r}_2) = \tau(\mathbf{r}_1|\mathbf{r}_2) - \tau(\mathbf{r}_2|\mathbf{r}_1)$ to an internal steady flow $\mathbf{v}(\mathbf{r})$. The motivation for this study is the interpretation of travel times measured between points that are separated by large angular distances (see e.g. [3]), which requires a setup in spherical geometry. The position vector in the solar interior, $\mathbf{r} = (r, \theta, \phi)$, is defined in a spherical-polar coordinate system. Under the assumption that the magnitude of the flow is small, the relationship between \mathbf{v} and $\delta\tau$ is given by the following integral equation:

$$\delta\tau = \int_{\odot} \mathbf{K}(\mathbf{r}) \cdot \mathbf{v}(\mathbf{r}) d^3\mathbf{r}, \quad (1)$$

where the integral is over the entire volume of the Sun. The sensitivity of $\delta\tau$ to $\mathbf{v} = (v_r, v_\theta, v_\phi)$ is given by the vector kernel $\mathbf{K} = (K_r, K_\theta, K_\phi)$.

The general method for the computation of travel-time kernels in the Born-approximation was given by Gizon & Birch [4]. This method was successfully applied by Birch et al. [5] to obtain sound-speed kernels in plane-parallel

geometry. Approximate kernels for sound-speed perturbations have also been calculated in spherical geometry in the single-source approximation by Birch & Kosovichev [6].

2. BACKGROUND SOLAR MODEL

The derivation of travel-time sensitivity kernels requires a background solar model. We used model S of Christensen-Dalsgaard et al. [7], which is spherically symmetric and contains no background flow.

In order to model the excitation of solar oscillations by convection, we use a stochastic forcing term uniformly distributed at a fixed depth of 76 km below the photosphere. This forcing function is the same as the one used by Birch et al. [5], with a correlation time of 68 s. It is assumed that the sources of excitation of the waves are spatially uncorrelated.

3. GREEN'S FUNCTIONS

The zero-order wavefield (in the absence of a flow) is obtained by convolving the forcing function with the zero-order Green's tensor [4]. By definition, the zero-order Green's function $G_{ij}(\mathbf{r}|\mathbf{r}'; t - t')$ gives the i -th component of the displacement vector at (\mathbf{r}, t) caused by an impulsive source at (\mathbf{r}', t') acting in the j -th direction [8, 5]. The Green's function can be expressed as a sum over adiabatic eigenfunctions of oscillation (complete basis), which were computed with the pulsation package ADI-PACK [9]. As a first step, we have used only modes with $l < 300$, where l is the spherical harmonic degree. Phenomenological mode damping was included in the momentum equation, and is consistent with the mode line widths measured by Schou [10] from one year of medium-degree MDI data.

Figure 1 shows an example Green's function, $G_{rr}(\mathbf{r}|\mathbf{r}'; t) = G_{rr}(\Delta, t)$, which gives the radial displacement at the surface (\mathbf{r}) caused by an impulsive radial displacement on the solar surface (\mathbf{r}'). This

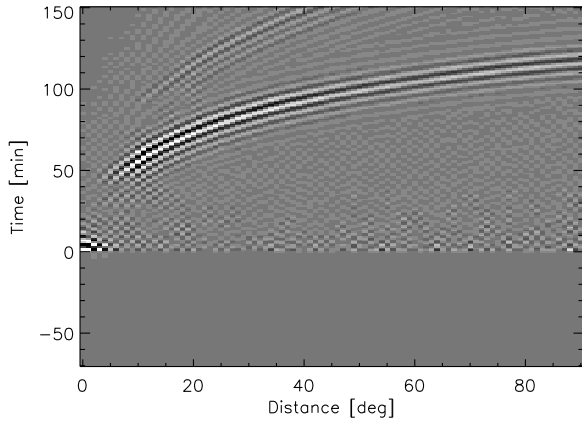


Figure 1. Green's function $G_{rr}(\Delta, t)$ as a function of angular distance, Δ , and time lag, t . Both the source and the observation points are on the solar surface. The amplitude of the Green's function was scaled by a factor proportional to Δ to bring out details at large angular distances and large time lags.

Green's function is shown as a function of the angular distance Δ between the source \mathbf{r}' and the observation point \mathbf{r} , measured along a great circle. By construction, the Green's function is causal (zero for $t < 0$). The main ridge of the Green's function follows the time-distance curve [2]. The second ridge at later times corresponds to waves that bounce once in between the source and the observation point. We note that the effects of mode damping on the Green's function are quite significant.

4. ZERO-ORDER POWER SPECTRUM AND CROSS-COVARIANCE

The expectation value of the power spectrum of the observed signal depends on the Green's tensor and on the source covariance matrix. In addition, it depends on what signal is being observed. For the sake of simplicity, we choose the radial component of velocity at the photosphere as the observable. The instrumental point-spread function of the telescope may be included by applying a low pass filter on the spatial transform of the signal; we took a filter of the form $\exp[-(l/150)^2]$ to model MDI in its medium-degree resolution mode.

Figure 2 shows the power spectrum of the radial component of velocity. Overall, the power is quite close to the real observations, although it could still be improved. The jagged appearance at high frequencies is due to missing modes, i.e. modes for which we did not have a linewidth measurement; this could easily be fixed in the future by extrapolation. Figure 3 is a cut through this power spectrum at spherical harmonic degree 30. The fact that power peaks near 3 mHz indicates that the source function that drives the oscillations is reasonable.

The model cross-covariance function is shown in Fig. 4b

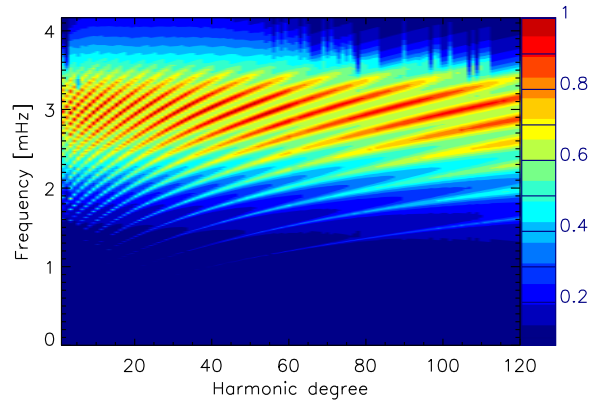


Figure 2. Power spectrum of the radial component of velocity as a function of harmonic degree and temporal frequency. The color scale gives the natural logarithm of the power.

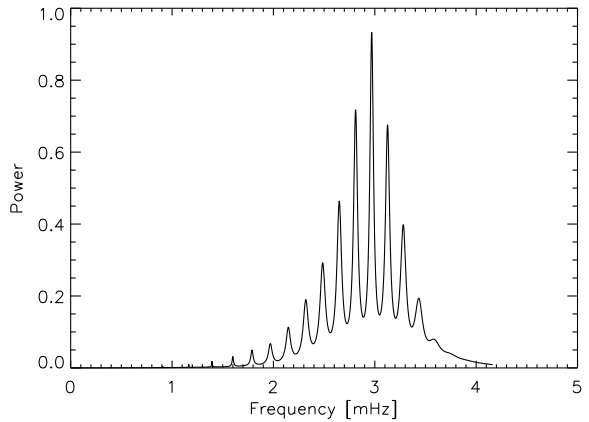


Figure 3. Cut through the power spectrum of Fig. 2 at $l = 30$, versus temporal frequency.

at fixed angular distance $\Delta = 30^\circ$, as a function of correlation time lag. Only the first-bounce correlations are shown. For comparison, an observed cross-covariance function is shown in Fig. 4a (courtesy of J.G. Beck). The agreement between theory and observation is not perfect, but reasonably good for our current purpose.

5. UNIFORM ROTATION

We first study the effect of uniform rotation on the cross-correlation and the travel times. In this case, the vector flow is of the form

$$\mathbf{v}(\mathbf{r}) = r\Omega \sin \theta \hat{\phi}, \quad (2)$$

where Ω is the angular velocity. Given two points \mathbf{r}_1 and \mathbf{r}_2 on the equator and separated by an angular distance Δ , the cross-covariance between these two points is given by

$$C(\Delta, t) = C_0(|\Delta - \Omega t|, t), \quad (3)$$

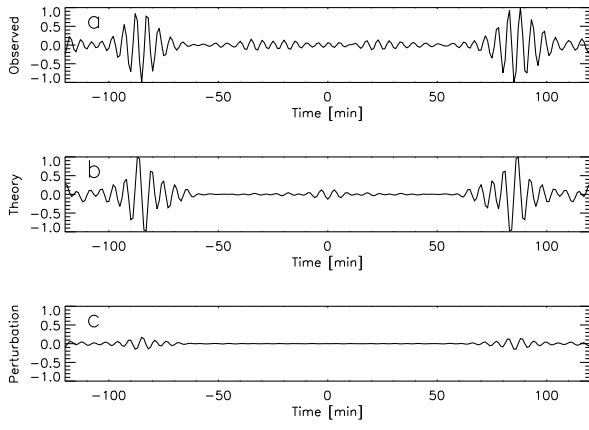


Figure 4. Cross-covariance functions at angular distance $\Delta = 30^\circ$ as a function of correlation time lag. (a) Observed cross-covariance using MDI medium-degree data, according to the procedure described by Giles [3]. (b) Theoretical cross-covariance from the present work. (c) Theoretical perturbation to the cross-covariance caused by uniform rotation with $\Omega/2\pi = 430$ nHz. The two observation points are on the equator.

where C_0 is the zero-order cross-covariance function (no rotation). The above equation was obtained by transforming from an inertial frame to the co-rotating frame. It is valid if no spatial filtering is applied to the observed signal.

Figure 4c shows the perturbation to C_0 when $\Omega/2\pi = 430$ nHz, i.e. the difference $\Delta C = C_0(|\Delta - \Omega t|, t) - C_0(\Delta, t)$. The function $\Delta C(\Delta, t)$ is nearly antisymmetric in t . This is consistent with the idea that rotation affects mostly the travel-time difference ($\delta\tau$), not predominantly the mean travel time.

We have measured the first-bounce travel-time difference according to the definition given by Gizon & Birch [11]. As can be seen in Fig. 5, the dependence between $\delta\tau$ and Ω is almost linear in the range $-500 < \Omega/2\pi < 500$ nHz. This provides some justification for wanting to obtain linear sensitivity kernels, as defined by Eq. (1).

6. KERNELS FOR FLOWS

The basic method for computing travel-time sensitivity kernels was developed by geophysicists, using a single-scattering approximation (e.g. [12]). The same method was adapted by Gizon & Birch [4] in the context of helioseismology, using the first Born approximation and taking into account the fact that waves are generated by random sources that are distributed in the near-surface layers of the Sun. It is relatively straightforward to apply this procedure to obtain an expression for sensitivity kernels for flows, in spherical geometry. Using the notations of Gizon & Birch [4], the first-order perturbation to the wave displacement, $\delta\xi$, is related to the flow, v , according to

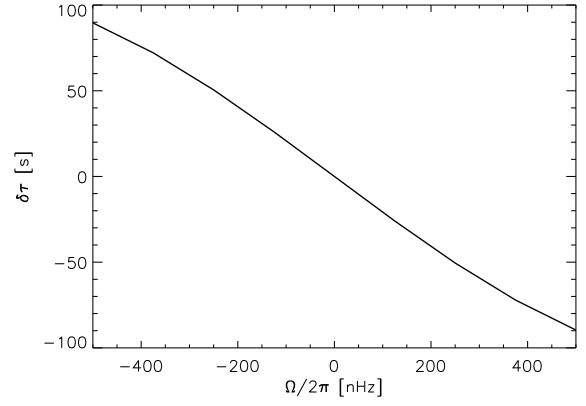


Figure 5. Travel-time difference $\delta\tau$ due to uniform rotation (angular velocity Ω). The two observation points are on the equator, separated by the angular distance $\Delta = 30^\circ$.

$L_0[\delta\xi] = -2\rho v \cdot \nabla \partial \xi_0 / \partial t$, where L_0 is the zero-order (i.e. no-flow) wave operator, ξ_0 is the zero-order wave displacement, and ρ is the density. The first Born approximation is an equivalent-source description of wave interaction: we can solve for $\delta\xi$ by using the unperturbed Green's tensor discussed in Section 3. We have ignored the first-order effect of vertical flows on the radial stratification.

The numerical evaluation of the kernels, however, is not trivial: it requires large computer resources. As a start, we have chosen to consider the case when only modes with fixed values of the harmonic degree l and the radial order n enter the expression of the kernels. This is meant to represent the case when the observed signal is filtered to let through only this particular multiplet. The flows only couple the $2l + 1$ azimuthal orders, m .

Figure 6 shows cuts through a kernel K_ϕ (sensitivity to v_ϕ), which only includes contributions from the modes with $l = 30$ and $n = 10$. The kernel has maximum values close to the observation points and near the surface. In addition, there is some sensitivity on the opposite side of the Sun (Single-multiplet kernels are invariant under the transformation $\phi \rightarrow \phi + \pi$). Elliptical and hyperbolic features are seen in the cut $r = R_\odot$, consistent with geometrical features seen in other kernels [4, 5]. As expected, the sensitivity reaches a depth that matches the lower turning point of the modes' eigenfunctions.

In order to check if the overall scaling of the above kernel is correct, we compute the travel-time difference due to uniform rotation in two different ways: (1) by integrating $rK_\phi \sin \theta$ over the volume of the Sun and (2) by measuring the travel times from the perturbed cross-covariance according to Eq. (3). The comparison between (1) and (2) is shown in Fig. 7. The agreement is found to be good.

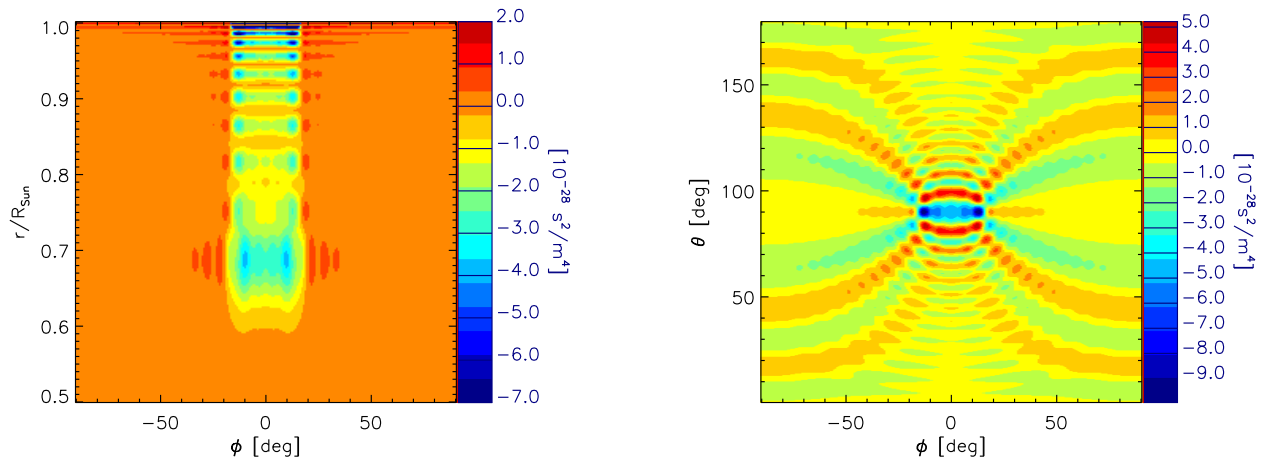


Figure 6. Cuts through a sensitivity kernel $K_\phi(r, \theta, \phi)$ in the case when only modes with $l = 30$ and $n = 10$ are observed. The kernel K_ϕ gives the sensitivity of the travel-time difference, $\delta\tau$, to the longitudinal component of the flow, v_ϕ . The observation points are on the equator ($\theta_1 = \theta_2 = \pi/2$) at longitudes $\phi_1 = -15^\circ$ and $\phi_2 = 15^\circ$, separated by the angular distance $\Delta = \phi_2 - \phi_1 = 30^\circ$. Left: Cut through K_ϕ at $\theta = \pi/2$ (equator). Right: Cut through K_ϕ at $r = R_\odot$. Only half of the kernel is shown in these two plots: the full kernel is symmetric with respect to the center of the Sun. The values of the kernel are in the range $[-36.4, 7.3] \times 10^{-28} \text{ s}^2 \text{ m}^{-4}$.

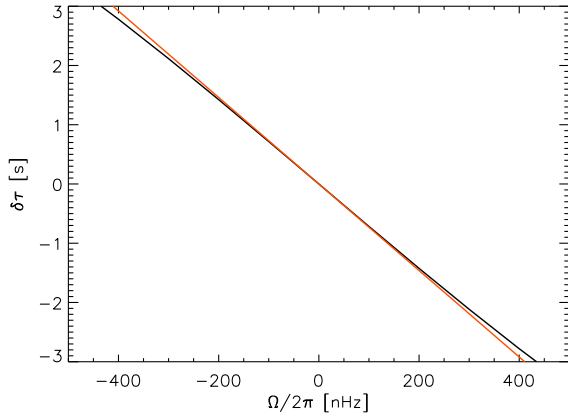


Figure 7. Travel-time difference $\delta\tau$ due to uniform rotation, in the case when only modes with $l = 30$ and $n = 10$ are observed. The two observation points are on the equator, separated by the angular distance $\Delta = 30^\circ$. The black line is for the exact answer, while the red line is obtained by integrating $rK_\phi \sin \theta$ over the volume of the Sun, where K_ϕ is the kernel shown in Fig. 6.

7. FUTURE WORK

We have set up the general problem of the computation of travel-time sensitivity kernels for flows, in spherical geometry. Simple tests have been performed on kernels when a single multiplet (n, l) is present. The full kernel includes several sums over all the modes, including couplings terms. Although our code is ready for this calculation, we are currently limited by computer resources. An efficient implementation of the code will be required

in order to speed up the calculation. We suspect that a number of physical approximations will have to be used as well. Additional effects, like foreshortening and the projection of the surface velocity onto the line of sight, are, in principle, conceptually easy to implement.

REFERENCES

- [1] Duvall T.L., Jefferies S.M., Harvey J.W., Pomerantz M.A., 1993, Nature, 362, 430
- [2] Kosovichev A.G., Duvall T.L., Scherrer P.H., 2000, Solar Physics 192, 159
- [3] Giles P., 1999, Probing Flows in the Upper Convection Zone, Ph.D. thesis, Stanford University
- [4] Gizon L., Birch A.C., 2002, ApJ, 571, 966
- [5] Birch A.C., Kosovichev A.G., Duvall T.L., 2004, ApJ 608, 580
- [6] Birch A.C., Kosovichev A.G., 2000, Solar Physics 192, 193
- [7] Christensen-Dalsgaard J. et al., 1996, Science 272, 1286
- [8] Dahlen F.A., Tromp J., 1998, Theoretical Global Seismology, Princeton Univ. Press
- [9] Christensen-Dalsgaard J., Berthomieu G., 1991, in Solar interior and (Univ. Arizona Press), 401
- [10] Schou J., 2006, private communication
- [11] Gizon L., Birch A.C., 2004, ApJ, 614, 472
- [12] Zhao L., Jordan T.H., 1998, Geophys. J. Int., 133, 683